Desalination and Water Treatment
www.deswater.com

doi: 10.5004/dwt.2020.24862

174 (2020) 63–70
January

Optimization of the evaporation step in cellulose acetate membranes preparation by dry–wet phase inversion technique for water desalination applications

Amira S. Mohammed Ali*, Eman A. Fadl, Moataz M. Soliman, Sherif H. Kandil

Materials Science Department, Institute of Graduate Studies and Research (IGSR), Alexandria University, 163 Horrya Avenue, El-Shatby, P.O. Box: 832, Alexandria, Egypt, emails: amira.mali@alexu.edu.eg (A.S. Mohammed Ali), eman_fadl@yahoo.com (E.A. Fadl), msoliman@alexu.edu.eg (M.M. Soliman), s.kandil@usa.net (S.H. Kandil)

Received 9 June 2018; Accepted 5 September 2019

ABSTRACT

In this study, cellulose acetate (CA) membranes were prepared by the dry-wet phase inversion technique for desalination application. The effect of evaporation time on the properties of the prepared cellulose acetate membrane has been investigated. Different evaporation time was selected such as (30, 60, 90 and 120 s). The membrane characterization was carried out by using Fourier transform infrared (FTIR) analysis, scanning electron microscopy (SEM), contact angle measurements. Brackish water was used as a feed solution in a cross flow unit to evaluate the membrane performance. The effect of the evaporation time on the membrane's water flux and salt rejection was tested. The results showed that the different evaporation time has affected the structure as deduced by the FTIR analysis. The SEM analysis showed the asymmetric CA membranes structure, where a thin dense selective barrier layer was deposited (in a finger-like structure) on the surface of the prepared membranes. As the evaporation time increased, the thickness of this layer has increased and the value of the contact angle has decreased. The highest rejection, obtained from the membrane that was prepared with the evaporation time 60 s, reached 96.5% salt rejection with a relatively low flux of 1.0234 L/m^2 h.

Keywords: Cellulose acetate membrane; Reverse osmosis; Evaporation time; Phase inversion; Water desalination

1. Introduction

The global demand for water is expected to increase by 30% by the year 2030. Some investigators foresee that accessible water supplies will fulfill just 60% of the demand at that time, perhaps less [1]. In the Arab Region, the majority of its countries are situated in areas that are considered as one of the world's most water-stressed regions that have limited availability of renewable fresh water. Hence water scarcity is one of the most pressing challenges facing the Arab countries, displaying a substantial danger that could contrarily affect the financial improvement endeavors [2]. Egypt is one of these countries that have water scarcity problem [3]. To produce fresh water, desalination is needed, which is a separation process for removing dissolved salts and other minerals from various water sources, such as seawater and brackish water [4].

Reverse osmosis membrane manufacturing is one of the core element technologies in desalination industry. There are two types of RO membranes: cellulose acetate (CA) asymmetric membrane and thin-film composite (TFC) membrane. Nowadays, the TFC membrane is widely used in RO processes due to its low energy consumption and good permselectivity. CA membranes have been partially used for their excellent tolerance for chlorine ions and micro-organisms [4]. However, CA membranes have a technical limitation which is their relatively low water flux [4].

---

* Corresponding author.

Phase inversion is one of the most versatile and cost-effective membrane fabrication techniques for the preparation of polymeric membranes in a wide range of pore sizes with various hydrophilic/hydrophobic and charged properties at high values of average porosity [5]. The membrane prepared with the phase inversion process is affected by the choice of polymer, the choice of solvent and nonsolvent, composition of the casting solution, composition of the coagulant bath, gelation and crystallization behavior of the polymer, temperature of the casting solution and the coagulation bath as well as the evaporation step [5]. If one or more of these parameters change, the membrane structure can change from a very open porous form to a very dense structure; as these parameters are not independent on each other [6].

In this work, the evaporation time, being one of the key parameters in the preparation of cellulose acetate membranes for RO, has been chosen for a "novel" system composed of cellulose acetate, acetone, dioxane, methanol and acetic acid. The effect of the evaporation time was investigated on the membrane characteristics; structure, hydrophilicity, and membrane performance; mainly the salt rejection and water flux using salt water with 10,000 ppm sodium chloride. The chosen evaporation times were 30, 60, 90, 120 s, membranes with evaporation time less than 30 s (7 and 15 s) were prepared, but when they were subjected to the applied pressure; they got ruptured during the investigation steps.

2. Experimental work

2.1. Materials

Cellulose acetate was obtained from Across Company (Belgium) with 39.8% acetyl content and its average number molecular weight was 100,000 Da. Acetone and dioxane were used as solvents. Acetone was purchased from Fisher Scientific Company (United States), and dioxane was purchased from Cambrian Chemical Company (Canada). Acetic acid was used as a softener and was purchased from Carlo Erba reagent SPA Inc., (France). Methanol was used as a nonsolvent in CA membrane preparation, and was purchased from Carlo Erba reagent SPA Inc. Sodium chloride (NaCl) was used to form a simulated saline water solution with 10,000 ppm sodium chloride, and was purchased from MP Biomedicals, LLC, France. All chemicals and solvents of analytical grade were used as received.

2.2. Methods

2.2.1. Preparation of cellulose acetate membranes

CA-RO membranes were prepared from a homogeneous solution composed of CA (14 wt%), acetone (17.5 wt%), dioxane (45.9 wt%), methanol (13.9 wt%) and acetic acid (8.6 wt%), then the solution was stirred using a magnetic stirrer and left overnight then cooled to 4°C. The solution was casted using an automatic micrometer applicator with (250 µm clearance gap) on a clean glass plate at room temperature. The solvents were allowed to evaporate within different durations (30, 60, 90 and 120 s), the membranes were given the names M30, M60, M90 and M120 were the number refers to the evaporation time. Then the cast films were immersed into a 4°C water bath and were kept for 2 h. The coagulated membranes were washed using deionized water, then the prepared membranes were thermally annealed by immersion in a hot water bath of 80°C–85°C [7], and they were held for 10 min, to consolidate the dense layer which provides the high solute rejection of such membranes [8].

2.2.2. Cellulose acetate membrane characterization

The functional groups of the prepared CA membranes were analyzed using Fourier transform infrared spectroscopy (FTIR spectrum BX 11 spectrometer FTIR LX 18-5255 PerkinElmer, United States). The surface morphology of the membranes was studied using scanning electron microscopy (SEM). Samples were prepared as follows: the dried membranes were cut under liquid nitrogen and mounted on a brass plate. The membranes were then sputter-coated with a thin film of gold. The surface and the cross-sectional images of the membranes were obtained using (Jeol JSM 5300, Japan) scanning electron microscope. AFM images were carried out by taking a sample with dimensions of 1 × 1 µm, 5 × 5 µm and 10 × 10 µm, using SPM-9700, Shimadzu, (Japan), equipped with dynamic mode at ambient temperature. A microcantilever OMCL-TR800PSA (Olympus, Japan) was used.

The hydrophilicity measurements of the CA-RO membranes surfaces were measured using Rame-Hart, Instrument Company, France. A drop of distilled water (2 µL) was placed on the membrane surface (3 cm × 2 cm) using micro syringe (Hamilton Company, Reno, NV). The contact angle was measured within 30 s after the water drop was placed. To improve the statistics of the contact angle measurement, each reported data point is the average of five measurements at different positions and at the same condition.

2.2.3. Lab-scale RO performance test

The performance measurements were carried out using reverse osmosis cell which consists of a commercially available cross-flow stainless steel CF042 cell (with a membrane area of 42 cm^2), and a hydraulic pump of a maximum pressure 69 bar, with a pressure control valve and gauge through the rejection line. A flow meter F-550 (USA) was connected to obtain a constant flow of 1 L/min. Fig. 1 shows a schematic diagram for the reverse osmosis cell that was used throughout the experiments of the membrane evaluation.

Prior to introducing the saline feed water, the membranes were flushed in the RO system with deionized water for 30 min until a steady permeate flux was achieved, then the saline water was introduced, where each filtration run was operated under contact-pressure mode. The RO performance experiments were conducted with an initial feed concentration of NaCl (10,000 ppm). The pH and the temperature of the feed solution were kept constant at 7°C and 25°C, respectively. The test samples were taken from the feed and permeate every 10 min for analysis. The concentrations were determined using the TDS meter (430 portable, Jenway, England). The pure water flux was calculated using the following equation:

$$\text{Flux} = \frac{Q}{A \times \Delta t} \tag{1}$$

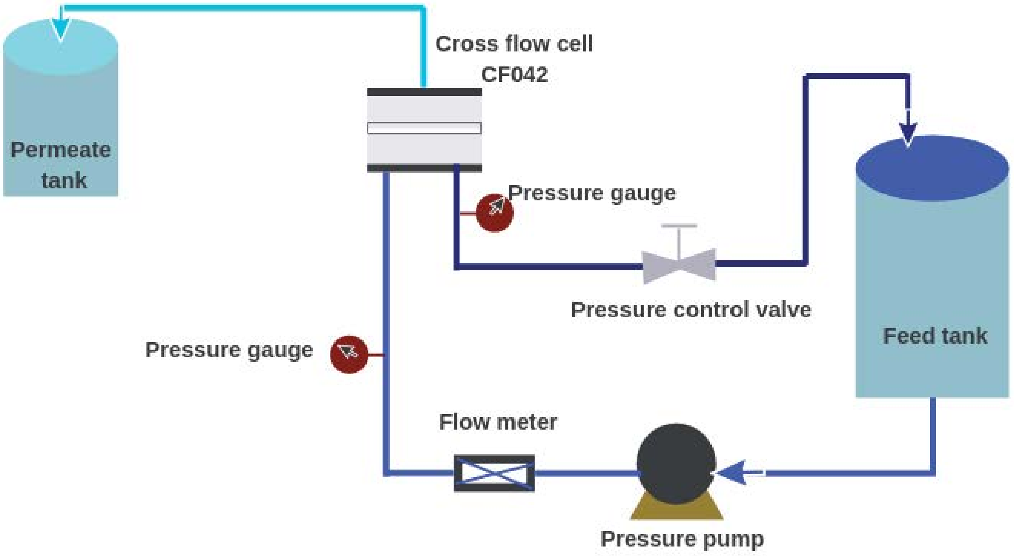

Fig. 1. Schematic diagram for the cross-flow reverse osmosis unit.

where Q is the volume of permeate (L), A is the effective membrane area (m^2) and Δt is the sampling time (h) [9].

The percentage salt rejection (SR) is calculated using the following equation:

$$\text{SR}\,\% = \left[\frac{\left(C_f - C_p\right)}{C_f}\right] \times 100 \qquad (2)$$

where C_f is the feed concentration and C_p is the permeate concentration [10].

3. Results and discussion

3.1. Effect of evaporation time on the CA membrane structure

During the evaporation step, the solvent goes out of the casted membrane surface, thus increasing the polymer concentration at the top surface layer of the membrane and induces a denser surface layer. The prepared membranes with evaporation time less than 30 s were ruptured during the operation. The membranes were tested for evaporation times that varied from 30 to 120 s to investigate the effect of the evaporation time. The membranes were denoted according to the evaporation time as (M30, M60, M90 and M120). The FT-IR has been used as a useful tool for determining the specific functional groups or chemical bonds that existed in the membrane material. Fig. 2 shows the FT-IR spectra of the prepared membranes.

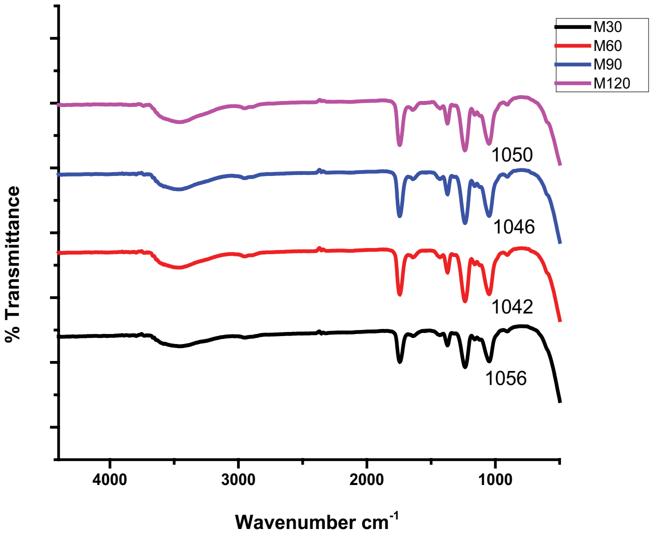

Fig. 2. FT-IR spectra of CA membranes prepared at different evaporation durations M30, M60, M90 and M120.

There is a broad band at 3,484 cm^{-1} which is assigned to the stretching vibration of the OH. The peak at 2,940 cm^{-1} represents the aliphatic C–H group, the peak around 1,748 cm^{-1} is attributed to the stretching vibration of the C=O bond of the aldehyde of CA. The peak at 1,636 cm^{-1} represents free water molecule (water of crystallization), and the peak around 1,512 cm^{-1} is attributed to the stretching mode of the C=C bond. The characteristic peak around 1,434 cm^{-1} represents the bending vibration of CH$_2$. The peak around 1,372 cm^{-1} shows the O–H bending vibration, while the peak around 1,234 cm^{-1} is assigned to the stretching vibration of the C–O group, and the peak at 1,054 cm^{-1} represents the C–O–C ether linkage from the glycoside unit, and finally the peak at around 908 cm^{-1} corresponds to the out-of-plane C–H bend (pyranose ring) [11–14]. There is a slight change in the IR spectra of the CA membranes prepared at different evaporation durations, for example the wavenumber shift of the ether group C–O–C was present in the range 1,040–1,056 cm^{-1}. This is due to the different packing structures of the prepared membranes resulting from different evaporation durations. Also for the –OH peak, as the evaporation time increases, it became more pronounced and more intense; for example, in the M30 and M120 spectrum. It can be suggested that the wavelength change will be reflected in the membrane performance; this is in a good agreement with the work done by Kusworo et al. [15].

3.2. Effect of evaporation time on the CA membrane morphology

The SEM images of the surface, cross-section and bottom of the prepared membranes are presented in Fig. 3. All the structures of the membranes consist of a dense skin layer (air side) which acts as a barrier responsible for the salt rejection. It was supported by a spongy structure separated by finger-like porous substructure, which acts as a mechanical support for the membrane. The surface of the CA membranes shows a ridge and valley structure. The morphological studies of the membrane surfaces showed a decrease in surface roughness as the evaporation time increases.

It is noticed that the ridges and valleys of the M120 surface are broader and wider than other membranes, and its surface has less roughness than the membranes prepared with evaporation times less than 120 s. This difference in surface morphology and surface roughness were affected by the evaporation time.

The thickness of the membrane dense layer was also affected by the evaporation time. During the evaporation step, the solvent goes out of the casted membrane surface, thus increasing the polymer concentration of the top surface layer in the membrane. The cross-section membrane morphologies show that, as the evaporation time increases, the thickness of the thin selective layer increases. Similar results were found by Choi et al. [16]. Fig. 4 shows the variation of thickness of the selective dense layer for the membranes prepared at different evaporation time. It was measured using SEM and by Digitizer software.

The cross-section morphology differed from one membrane to another. In our case, we chose a mixture of solvents and nonsolvent; acetone was used as a vaporizable conventional solvent for cellulose acetate, dioxane was used in order to have a homogeneous casting solution, acetic acid as used as a softener to improve the polymer mobility for the development of the polymer structure. As well as, during the coagulation, the acetic acid froze the structure through hydrogen bonding. Finally methanol was used as a nonsolvent for the cellulose acetate; it simulated the water absorption by the membranes and therefore, tend to increase their flow performance [17].

The finger-like tears in the membrane's cross section can grow only in the cast solution fluid lower layer as this fluid layer's thickness decreases with the increase in the solvent evaporation time before leaching [18]. The formation of finger-like tears, growing in the fluid layer, is generally associated with a high rate of precipitation [18–21]. At shorter evaporation time leads to instantaneous demixing while longer evaporation time leads to delayed demixing. When the solvent had evaporated, the concentration and the viscosity of the polymer solutions increased; thus, the solvent–nonsolvent exchange process is restricted [22]. That is why we can see finger-like tears structure in M30 membrane.

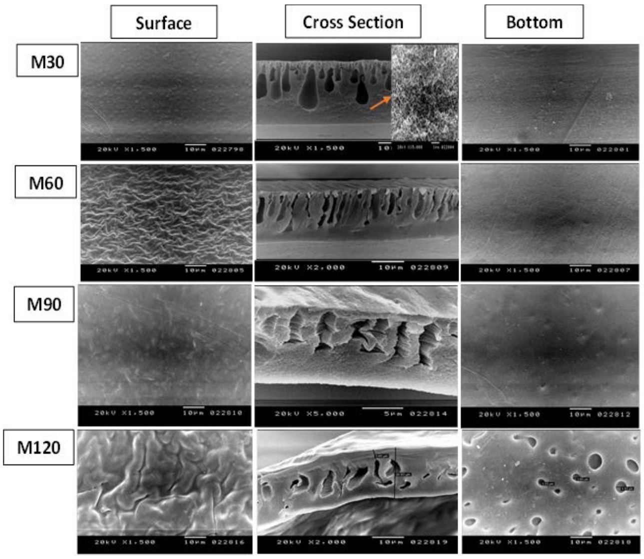

Fig. 3. Morphology of the CA membrane prepared with different evaporation time.

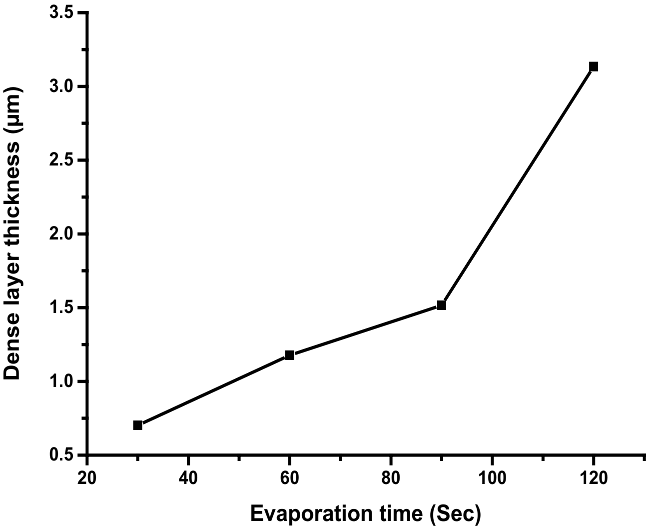

Fig. 4. Membranes' dense layer thickness at different evaporation time.

The M30 has finger-like tears separated by a sponge structure. The M60 has compacted fingers compared with M30, separated by thick walls. The M90 and M120 have broader fingers and thicker fingers walls. This difference in the cross-section morphology may be attributed to the skin layer thickness. As the skin layer thickness increases, the membrane cross section is more likely to be dense. This change in morphology is probably because the skin layer controls the nonsolvent and solvent exchange. When the skin layer thickness increases, the nonsolvent, that is, water finds it difficult to penetrate the membrane, and similarly the mixture of solvents also finds it difficult to diffuse of the membrane's skin. This situation leads to a slow demixing process and the produced membrane is likely to be dense. Similar interpretation was found by Saljoughi and Mohammadi [23].

The pores appearing on the bottom of the membrane start to appear on the M90 and become bigger and more pronounced on the bottom of M120. This may be due to the fact that the longer the evaporation time, the more concentrated layer of CA will be found on the surface, which is more detected on M90 and M120 membranes. Different shrinkage rates will be produced for the surface and the bottom during their immersion in water.

3.3. AFM analysis

For structure–morphology correlation purpose, the selected sample of CA membrane with evaporation time 60 s was subjected to AFM analysis as illustrated in Fig. 5 for M60 membrane. The bright and dark regions are the peaks and valleys, respectively. Ra represents the average roughness and Rz is the difference in height between the average of the five highest peaks and the five lowest valleys along the assessment length of the profile [24]. Ra of the CA M60 membrane is 245.733 nm, Rz is 1.966 μm. All the surface roughness parameters were calculated from the AFM images using an AFM software program. The surface roughness parameters represent high value of surface's roughness.

The change in the evaporation time had a small effect on the membranes' hydrophilicity as shown in Fig. 6. As the

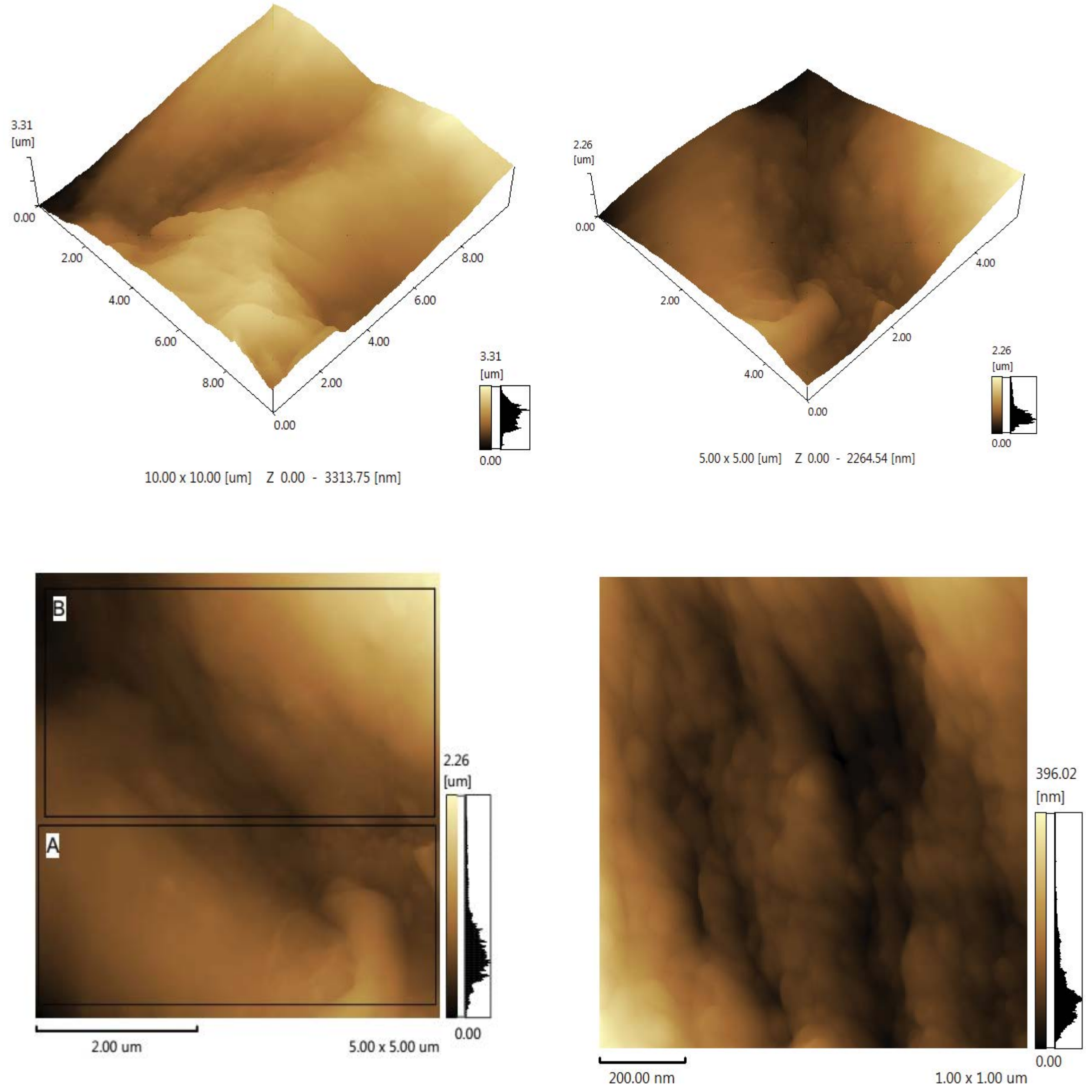

All Area		A		B	
LengthX	5.000[um]	LengthX	4.922[um]	LengthX	4.834[um]
LengthY	5.000[um]	LengthY	2.021[um]	LengthY	2.568[um]
Area	25.000[(um)2]	Area	9.949[(um)2]	Area	12.415[(um)2]
Ra	245.733[nm]	Ra	404.395[nm]	Ra	494.783[nm]
Rz	1.966[um]	Rz	1.293[um]	Rz	2.145[um]
Rzjis	961.667[nm]	Rzjis	613.632[nm]	Rzjis	1.021[um]
Rq	323.767[nm]	Rq	470.546[nm]	Rq	596.987[nm]
Rp	1.267[um]	Rp	1.189[um]	Rp	1.628[um]
Rv	699.031[nm]	Rv	103.639[nm]	Rv	516.834[nm]

Fig. 5. AFM analysis for CA M60 membrane.

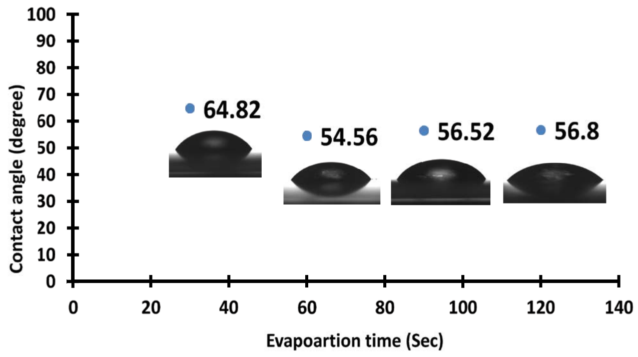

Fig. 6. Contact angle measurements for CA membranes prepared with different evaporation time.

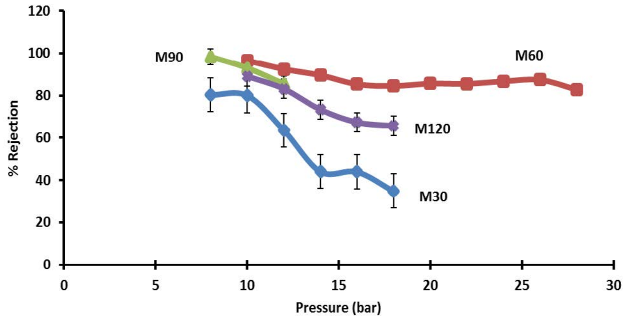

Fig. 7. Percentage rejection of different membranes prepared with different evaporation time and under different operating pressure.

evaporation time increases, the value of contact angle has decreased.

As mentioned above, the morphological studies of the membrane surfaces showed a decrease in surface roughness as the evaporation time increases, which may be contributed to the decrease of the contact angle measurements [25]. In addition, as the evaporation time increases, more solvent evaporates; consequently more polymer is concentrated at the top surface layer in the membrane, taking into consideration the hydrophilic nature of CA as a polymer, that is, CA concentration at the M120 surface is higher than the CA concentration at M30 surface. The higher the CA concentration at the surface, the lower the contact angle would be and hence the higher is the hydrophilicity [26].

The M30 had the highest contact angle among the others (64.82°), while M60 had the lowest contact angle (54.5°). The slight change in contact angle measurements between M60 and M120 is insignificant.

3.4. Effect of evaporation time on the CA membranes' performance

Figs. 7 and 8 show the performance of the prepared membranes (M30-M120) and indicate their stability with the applied pressure. Generally, the percentage salt rejection for all the membranes is decreasing with increasing the operating pressure. This is due to the concentration polarization phenomena, that is, the membrane fouling due to salt accumulation on its surface. The concentration polarization of the salt has many factors which may affect the desalination process. First of all, the osmotic pressure which must be exceeded is corresponding to the salt concentration at the membrane's surface and the concentration polarization allows that the effective osmotic pressure exceeds the bulk saline solution's osmotic pressure. As well as, concentration polarization affects the product water salinity because this salinity generally increases when the salt concentration at the surface of the membrane in the feed solution side increases [10,27].

From Fig. 7, at 10 bar, M60 produced the highest percentage salt rejection, while M30 has the lowest. The M60 case within the pressure ranging from 16 to 22 bar shows a stable profile salt rejection percentage that amounts to 85%. This is due to the compaction of the membrane's skin layer. This phenomenon could be attributed to the fact that as the pressure is applied, the Brownian movement of the polymer chains is restricted, and the structure of the polymer is compressed. The water within the amorphous region becomes more tightly bound, and so the membrane becomes more of an impenetrable barrier to sodium chloride [28].

It was observed that within the pressure range from 10 to 28 bar, the flux for all membranes is increasing with the increase in the transmembrane pressure as indicated in Fig. 8. This was due to the increase in the effective driving force (trans-membrane pressure) that is required for water permeation [24,29].

For all prepared membranes the permeate was obtained at 10 bar, so it has been taken as the reference pressure. From Fig. 7 it is obvious that the salt rejection has increased from

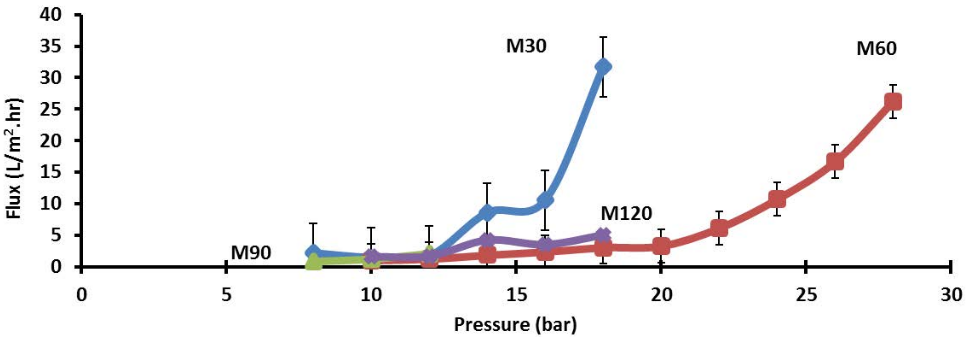

Fig. 8. Permeate water flux of CA membrane prepared with different evaporation time.

Table 1
Rupture pressure of the CA membranes prepared with different evaporation time

Membrane	Rupture pressure (bar)
M30	18
M60	28
M90	12
M120	18

80% to 96.5% for the membranes M30 and M60, respectively. This refers to the formation of a selective skin layer with a very small thickness (0.70 μm) for M30 that was not capable of having high salt rejection [30,31]. This thickness also leads to a comparatively high flux for M30 (1.428 L/m^2 h) as the thin selective layer facilitates water penetration. Although, the M60 membrane has achieved the highest salt rejection among the prepared membranes, its flux had the lowest value among other membranes (1.0234 L/m^2 h). This may be due to the formation of a relatively dense thick selective skin layer (1.177 μm) on the M60 surface, which has a pronounced effect on the membrane properties.

The effect of the membranes morphology is clear on the M60's performance and strength, whereas the finger-like sponge structure acted as a good support layer improving the membrane's mechanical strength that tolerated the pressure up to 28 bar. Meanwhile the M30 membrane did not tolerate the pressure more than 18 bar. This is probably due to the presence of the weak active dense thin layer, and the tear-like shape in the cross-section structure that acts as a weak spot vulnerable for crack propagation during the application of high pressure. This leads to low compaction tolerance and reduces the mechanical stability. The M60 membrane endured maximum operating and rupture pressure of 28 bar indicating that M60 has the optimum properties in terms of mechanical strength and salt rejection compared with the other prepared membranes. The rupture pressure, illustrated in Table 1 was selected as a criterion for expressing the mechanical properties [32,33].

While the M90 and M120 membranes had a relatively thicker dense selective layer (1.516 and 3.134 μm, respectively), they were supposed to show better performance in terms of salt rejection. On contrast they showed a decrease in salt rejection (93.07% and 89.06%, respectively), compared with the percentage salt rejection of M60 (96.55%). They, however produced higher flux (1.224 and 1.647 L/m^2 h, respectively) compared with M60 which produced 1.0234 L/m^2 h. The decrease in the salt rejection and the enhancement of water flux of the M90 and M120 membranes can be explained by the fact that the active thin layer becomes denser and thicker due to long evaporation durations, it does not tolerate the applied pressure, so it makes it easy for a crack to propagate in it, which results in the active layer distortion. Similar results were obtained by Gizli [34].

4. Conclusion

The evaporation time has proved to be an important parameter for determining the membrane characteristics; selectivity and pressure endurance as it affected the structure, morphology and hydrophilicity. As the evaporation time increases, the structure of the membrane tends to be denser, and the hydrophilicity of the membranes increases. The appropriate evaporation time is necessary to produce high salt rejection. For a system composed of cellulose acetate, acetone, dioxane, methanol and acetic acid, it was suggested that the optimum evaporation time is 60 s to obtain high salt rejection (96.5%). Such membrane was composed of dense selective layer supported on a finger-like structure, which acts as a mechanical support for the membrane; hence; it tolerated the highest rupture pressure of 28 bar compared with other membranes.

Acknowledgment

The authors would like to thank the Science and Technology Development Fund (STDF) in Egypt for supporting this work through the project entitled "Nanocomposite Thin Film Membranes Based on Polymers and Clays for Reverse Osmosis Utilizations", project ID: 3988.

References

[1] D.M. Stevens, J.Y. Shu, M. Reichert, A. Roy, Next-generation nanoporous materials: progress and prospects for reverse osmosis and nanofiltration, Ind. Eng. Chem. Res., 56 (2017) 10526–10551.

[2] W.K. Al-Zubari, In: The Water, Energy, and Food Security Nexus in the Arab Region, Springer, 2016, pp. 2–4.

[3] S.K. Sikdar, A. Criscuoli, In: Sustainable Membrane Technology for Water and Wastewater Treatment, Springer, 2017, pp. 4.

[4] D. Li, H. Wang, In: Functional Nanostructured Materials and Membranes for Water Treatment, Wiley-VCH Verlag GmbH & Co. KGaA, 2013, p. 163.

[5] B.S. Lalia, V. Kochkodan, R. Hashaikeh, N. Hilal, A review on membrane fabrication: structure, properties and performance relationship, Desalination, 326 (2013) 77–95.

[6] J., Mulder, Basic Principles of Membrane Technology, Springer Science & Business Media, 2012, p. 86.

[7] A. Morsy, S. Ebrahim, E. Kenawy, T. Abdel-Fattah, S. Kandil, Grafted cellulose acetate reverse osmosis membrane using 2-acrylamido-2-methylpropanesulfonic acid for water desalination, Water Sci. Technol. Water Supply, 16 (2016) 1046–1056.

[8] R. Matz, The structure of cellulose acetate membranes 1. The development of porous structures in anisotropic membranes, Desalination, 10 (1972) 1–15.

[9] H. Wu, B. Tang, P. Wu, Optimizing polyamide thin film composite membrane covalently bonded with modified mesoporous silica nanoparticles, J. Membr. Sci., 428 (2013) 341–348.

[10] J. Kucera, Reverse Osmosis Design, Processes, and Applications for Engineers. 2010. Co-published by John Wiley & Sons, Inc. Hoboken, New Jersey, and Scrivener Publishing LLC, Salem, Massachusetts, p. 23.

[11] A. Sabir, A. Islam, M. Shafiq, A. Shafeeq, M.T.Z. Butt, N.M. Ahmad, K. Sanaullah, T. Jamil, Novel polymer matrix composite membrane doped with fumed silica particles for reverse osmosis desalination, Desalination, 368 (2015) 159–170.

[12] V.K. Gupta, D. Pathania, P. Singh, B. S. Rathore, P. Chauhanc, Cellulose acetate–zirconium (IV) phosphate nano-composite with enhanced photo-catalytic activity, Carbohydr. Polym., 95 (2013) 434–440.

[13] M. Ali, M. Zafar, T. Jamil, M. Taqi, Z. Buttb, Influence of glycol additives on the structure and performance of cellulose acetate/zinc oxide blend membranes, Desalination, 270 (2011) 98–104.

[14] F.S. Dehkordi, M. Pakizeh, M.N. Mahboub, Properties and ultrafiltration efficiency of cellulose acetate/organically modified Mt (CA/OMMt) nanocomposite membrane for humic acid removal, Appl. Clay Sci., 105 (2015) 178–185.

[15] T.D. Kusworo, Budiyono, A.I. Wibowo, G.D. Harjanto, A.D. Yudisthira, F.B. Iswanto, Cellulose acetate membrane with improved perm-selectivity through modification dope composition and solvent evaporation for water softening, Res. J. Appl. Sci., Eng. Technol., 7 (2014) 3852–3859.

[16] H. Choi, S.H. Yoon, M. Son, E. Celik, H. Park, H. Choi, Efficacy of synthesis conditions on functionalized carbon nanotube blended cellulose acetate membrane for desalination. Desal. Wat. Treat., 57 (2016) 7545–7554.

[17] A.P. Duarte, M.T. Cidade, J.C. Bordado, Cellulose acetate reverse osmosis membranes: optimization of the composition, J. Appl. Polym. Sci., 100 (2006) 4052–4058.

[18] M.A. Frommer, R.M. Messalem, Mechanism of membrane formation. VI. Convective flows and large void formation during membrane precipitation, Ind. Eng. Chem. Prod. Res. Dev, 12 (1973) 328–333.

[19] D.M. Koenhen, M.H.V. Mulder, C.A. Smolders, Phase separation phenomena during the formation of asymmetric membranes, J. Appl. Polym. Sci., 21 (1977) 199–215.

[20] G.R. Guillen, G.Z. Ramon, H.P. Kavehpour, R.B. Kaner, E.M.V. Hoek, Direct microscopic observation of membrane formation by nonsolvent induced phase separation, J. Membr. Sci., 431 (2013) 212–220.

[21] Z. Li, C. Jiang, Investigation of the dynamics of poly (ether sulfone) membrane formation by immersion precipitation. J. Polym. Sci., Part B: Polym. Phys., 43 (2005) 498–510.

[22] I. Syahbanu, B. Piluharto, S. Khairi, Sudarko, Effect of Evaporation Time on Separation Performance of Polysulfone/Cellulose Acetate (PSF/CA) Membrane. in IOP Conference Series: Materials Science and Engineering, 2018, IOP Publishing, Conference 1, Vol. 299.

[23] E. Saljoughi, T. Mohammadi, Cellulose acetate (CA)/polyvinyl-pyrrolidone (PVP) blend asymmetric membranes: preparation, morphology and performance, Desalination, 249 (2009) 850–854.

[24] S. Waheed, A. Ahmad, S.M. Khan, S. e-Gul, T. Jamil, A. Islam, T. Hussain, Synthesis, characterization, permeation and anti-bacterial properties of cellulose acetate/polyethylene glycol membranes modified with chitosan, Desalination, 351 (2014) 59–69.

[25] S.H. Woo, J. Park, B.R. Min, Relationship between permeate flux and surface roughness of membranes with similar water contact angle values, Sep. Purif. Technol., 146 (2015) 187–191.

[26] H. Rusli, S. Gandasasmita, M.B. Amran, Cellulose acetate–silica fume membrane: characterization and application for separation of starch and maltose, Iran. Polym. J., 22 (2013) 335–340.

[27] P.L.T. Brian, Concentration Polar zation in Reverse Osmosis Desalination with Variable Flux and Incomplete Salt Rejection, Ind. Eng. Chem. Fundam., 4 (1965) 439–445.

[28] C. Reid, E. Breton, Water and ion flow across cellulosic membranes, J. Appl. Polym. Sci., 1 (1959) 133–143.

[29] G. Arthanareeswaran, P. Thanikaivelan, K. Srinivasna, D. Mohana, M. Rajendrana, Synthesis, characterization and thermal studies on cellulose acetate membranes with additive. Eur. Polym. J., 40 (2004) 2153–2159.

[30] S. Loeb, S. Sourirajan, High flow porous membranes for separating water from saline solutions, 1964, Google Patents.

[31] L. Lee, A method of forming a porous cellulose acetate membrane, 1973, Google Patents.

[32] A. Bottino, G. Capannelli, S. Munari, Factors Affecting the Structure and Properties of Asymmetric Polymeric Membranes, In Membranes and Membrane Processes, E. Drioli, M. Nakagaki, Editors. 1986, Springer US: Boston, MA. pp. 163–178.

[33] K. Wang, A.A. Abdalla, M.A. Khaleel, N. Hilal, M.k. Khraishesh, Mechanical properties of water desalination and wastewater treatment membranes, Desalination, 401 (2017) 190–205.

[34] N. Gizli, Morphological characterization of cellulose acetate based reverse osmosis membranes by atomic force microscopy (AFM) effect of evaporation time, J. Chem. Chem. Technol., 5 (2011) 5.